

RESEARCH ARTICLE

Open Access



The displacement mechanism of the cracked rock – a seismic design and prediction study using XFEM and ANNs

Omer Mughieda^{1*} , Lijie Guo², Yunchao Tang³, Nader M. Okasha⁴, Sayed Javid Azimi⁵, Abdoullah Namdar⁶ and Falak Azhar⁷

*Correspondence:
Omer Mughieda
omer.mughieda@adu.ac.ae

Full list of author information is
available at the end of the article

Abstract

Materials with sufficient strength and stiffness can transfer nonlinear design loads without damage. The present study compares crack propagation speed and shape in rock-like material and sandstone when subjected to seismic acceleration. The nonlinear extended finite element method (NXFEM) has been used in numerical simulation. It assumes the model has a pre-existing crack at 0° from the horizontal. The mechanical properties of the model, crack propagation shape, and crack speed were selected as the main parameters. The nonlinear stress and strain along the crack have been compared in two simulated models. NXFEM and Artificial Neural Networks (ANNs) were used to predict the displacement. The simulation results illustrate that the materials' crack propagation mechanism and mechanical properties control the stress, strain, and displacement at the selected points in the model. In addition, crack propagation in materials is related to elastic-plastic stresses and strains along the crack path. The speed and shape of the crack are associated with the mechanical properties of the materials. The prediction of crack paths helps to understand failure patterns. Comparison of the seismic response of the rock-like material with sandstone helps to assess the stress, strain, and displacement levels during cracking. This study's findings agree with the literature report and field observations.

Keywords Initial crack, Crack speed, Crack shape, Crack propagation, Displacement

Introduction

The initial crack types and propagation are unknown phenomena and require prediction to estimate a material's strength and stiffness. The prediction of cracking during an earthquake requires increased investigation. Predicting material failure caused by crack propagation due to seismic loading is essential for geotechnical engineering design. Prediction is also essential to reduce the impact of natural hazards on human life.

Experimental work has been reported on specimens made of rock-like material to study the crack coalescence path mechanism. A 2004 investigative study aimed to identify fracture resistance and crack initiation in offset rock joints. The tensile stress caused

crack initiation and propagation. The failure mode occurred because of the coalescence crack mechanism [1]. A study by Mughieda and Karasneh in 2006 investigated the application of biaxial loading to specimens of rock-like material to study the offset rock joints' coalescence crack path [2]. Furthermore, another study concluded that the size of the specimen impacts some experimental results, such as the mode of failure [3]. The prediction of crack propagation in sandstone is difficult to perform in the laboratory. Therefore, it requires NXFEM and statistical analysis. Simulation of exact seismic acceleration in the laboratory also requires hard work.

NXFEM has been used to investigate material fracture and crack propagation. The initial fracture in the earth structure causes differential displacement, different failure modes, shear stress, and shear strain. Experimental studies show that the seismic stability of the earth's structure is influenced and associated with the mechanical properties of the material [4–5]. Depending on loading and pre-existing crack inclination, rock cracks can be generally inclined at 0, 30, 45, 60, and 90 degrees [6]. In reality, the impact of the initial crack on the load response of different types of rocks remains unclear and requires further study. NXFEM is an advanced technique for predicting crack propagation in any material. This technique subjects the materials to nonlinear acceleration to contain the initial crack formed due to climate, material characteristics, or other reasons.

A rock mass usually has fractures [7], and a sandstone mass has varying mechanical properties [8]. Explaining fractures in sandstone is complicated, and it is not possible to explain them with a single equation. Sandstone has resilient characteristics and does not crack easily. Additionally, the phylitic in sandstone prevents cracks from developing easily [9]. Due to this sandstone characteristic, the present work assumed that the crack was not fully extended, and the extension occurred by applying seismic acceleration. Additionally, cracked sandstone seismic response was compared with a rock-like material.

In sedimentary basins, fracture modes are caused by fluid pressure and stress combinations [10–11]. The shape and amount of the occurring displacement are influenced by the rock's elastic properties and the applied load [12]. There is a need for further investigation and comparison with rock-like materials to better understand the variation in sandstone's crack propagation as a function of its mechanical properties.

A direct relationship exists between crack lengths and displacement when bedrock is subjected to a surcharge [13–14]. In the case of seismic acceleration, the displacement mechanism needs to be investigated in greater detail.

Numerous researchers have studied how to predict strength and failure in different geomaterials. For instance, studies have investigated the ultimate failure of flawed red sandstone specimens subjected to uniaxial compression [15–16]. Furthermore, strength and failure prediction has been reported for soil mixtures [17–18], soil compaction mechanism [19], concrete material fracture [20–22], materials crack assessment, and failure patterns [20–24]. Crack propagation prediction for specific earthen materials has also been carried out using experimental and numerical simulation [25]. In addition, numerical modeling has been reported on the buckling initiation, displacement, and deformation of natural rock, which leads to failure without considering crack initiation and propagation [26]. Crack propagation simulations of rock subjected to seismic acceleration are yet to be presented in the literature. In addition, the type of rock failure needs more study, considering the displacement, stress, and strain developing at critical

points in the rock. Moreover, the crack initiation, propagation, and stress-strain relationship along the crack need further investigation.

In the present study, a nonlinear numerical simulation has been performed to predict crack propagation by considering the initial crack, crack speed, and mechanical properties. To simulate the seismic response of the model, the displacement mechanism at selected points and the stress-strain relationship along the crack path in rock with a pre-existing crack were investigated. For displacement prediction, nonlinear numerical simulation and artificial neural networks (ANNs) were used. The findings of this study were compared with literature reports and field observations.

Simulation and materials

Figure 1 presents the entire investigation. Critical parts of the investigation include simulating the model's geometry with clear boundary conditions, selecting the appropriate theoretical concept for application in numerical simulation and statistical analysis, and collecting data for performing numerical simulation and statistical analysis. Numerical simulation, statistical analysis, field observation, and literature analysis were performed to predict the results.

The different types of cracks on the rock are shown in Fig. 2 [6]. A crack shape in the rock at 0° was selected for the present study. Rock-like materials and sandstone have been used for modeling. ABAQUS has been used for nonlinear simulation and to predict crack propagation. A pre-existing crack was assumed in half of the model in the simulation. The growing crack in the remaining half of the model has been investigated by considering the mechanical properties of the rock, applying seismic acceleration, the model's geometry, and the model's boundary conditions. The direction and propagation of the crack were predicted. For predicting displacement at the selected points of the model, nonlinear numerical simulation and artificial neural networks (ANNs) were used.

Table 1 shows the mechanical properties of the materials [7], which were used in the numerical simulation.

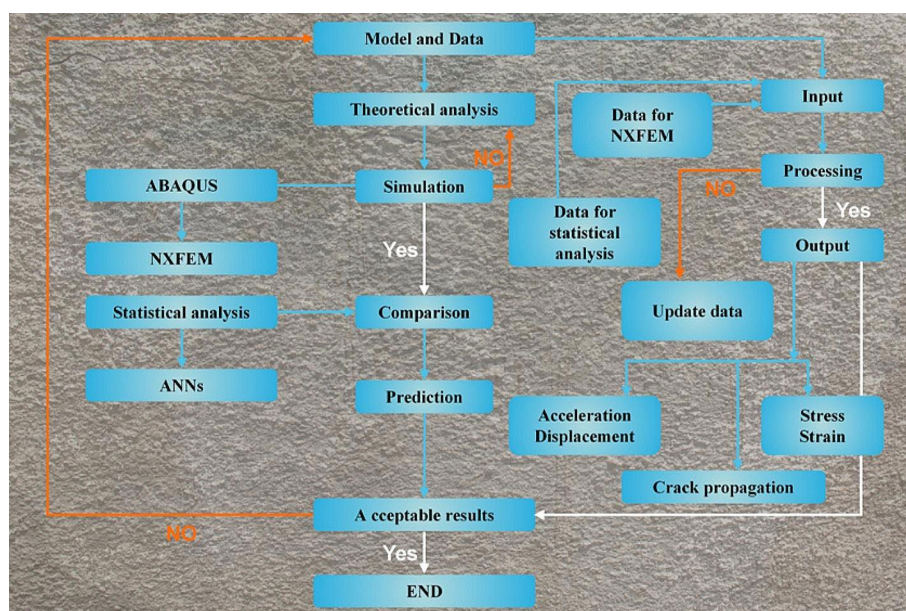


Fig. 1 The flowchart for prediction

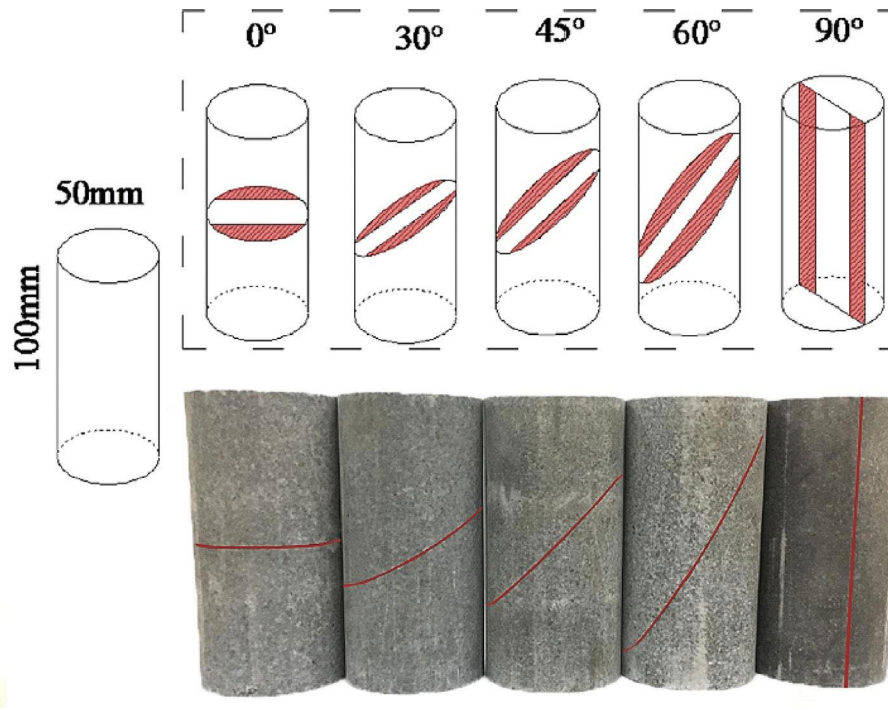


Fig. 2 The crack type on the rock with different angles [6]

Table 1 The mechanical properties of the rock-like material and sandstone [8]

Materials	Uniaxial compressive strength σ_c (MPa)	Tensile strength σ_t (MPa)	Elastic modulus E (GPa)	Poisson's ratio μ	Density ρ (g/cm ³)
Rock-like material	58.25	5.62	11.63	0.20	2.38
Sandstone	20~170	4~25	3~35	0.02~0.25	2.10~2.40

According to Fig. 2, the crack has different directions. Figure 3 shows the macrofracture on sandstone. In reference to Figs. 2 and 3, the crack in the laboratory simulation is similar to those that occur in nature. Figure 4 shows a 90-degree crack on the metasandstone specimens after performing the Brazilian Tensile Strength (BTS) test.

Figure 5 shows the crack in the rock. Cracks of this type have path directions of 0° and 90°. The figure depicts that either 0° or 90° cracks have propagated on the rock's surface, but the cracks have not reached the depth of the rock. The crack path at the end of the crack has a small opening. A numerical simulation has been done based on the pre-existing crack in the rock. It is assumed that the crack in models 1 and 2 pre-exists before applying seismic acceleration. This assumption is based on the direction of crack propagation observed in the field. This kind of crack impacts geotechnical engineering structural design. Pre-existing cracks in the present numerical simulation were straight before seismic loads were applied.

The geometry and boundary conditions of the model are shown in Fig. 6. The dimension of the model is 600 (mm) \times 600 (mm) \times 20 (mm), and the initial crack has a length of 300 (mm). All models have a similar geometry, but the mechanical properties are different for each model in numerical simulation. Models 1 and 2 have pre-existing open cracks of 0° at half the model length. Crack propagation in rock-like material and

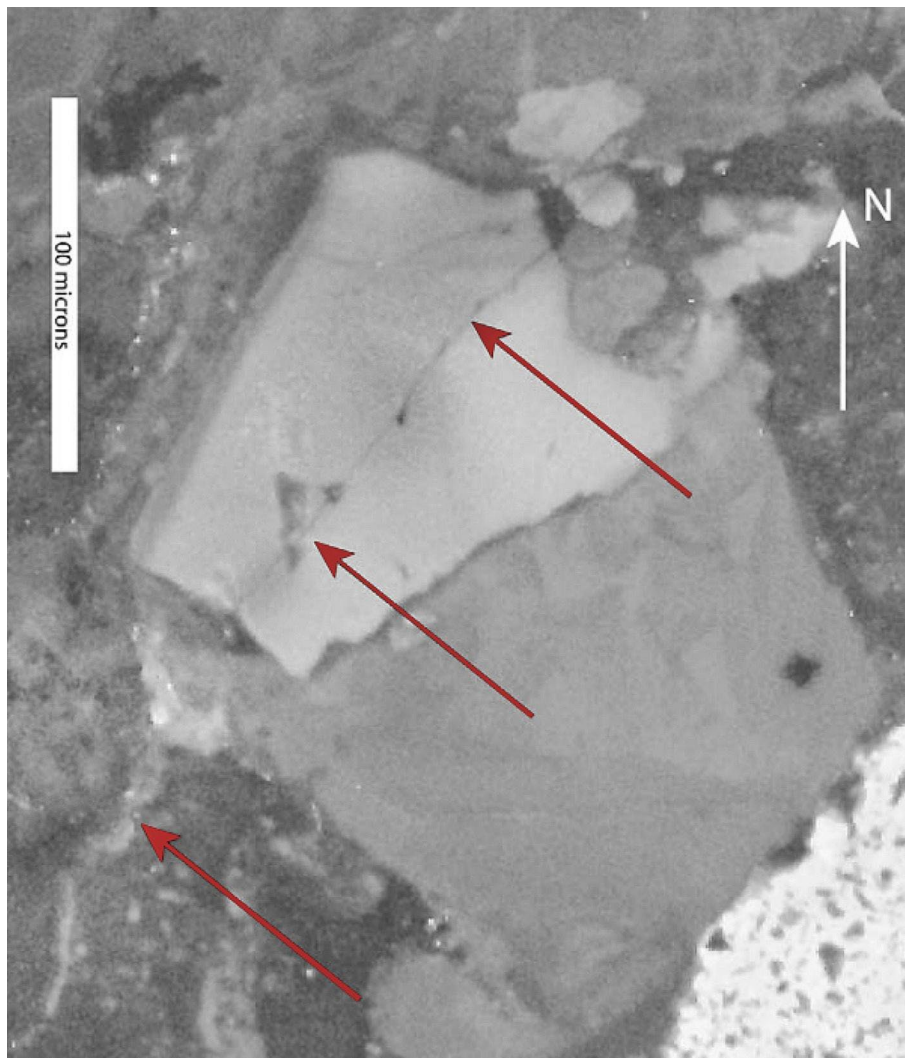


Fig. 3 The macrofracture on sandstone [9]

sandstone is compared. In addition, stress and strain along the crack path and displacement at selected points in the models have been predicted.

In Table 2, displacement (cm) and acceleration (g) in 0° , 90° , and 360° directions for the earthquake are shown for different distances from the epicenter. The Palekastro earthquake with 6.4 MWW has the highest acceleration (g) peak at -0.3432 (g). The earthquake occurred at 12:24:03 on 12 Oct 2021, with coordinates 35.1931 and 26.2556, at a depth of 10.0 km.

The information about this earthquake was recorded at the Town Hall Siteia Lassithi Crete earthquake station, located 13.6 km from the earthquake epicenter. The data recorded at the station was used to perform the numerical simulation presented in the current study. Figures 7 and 8 depict the seismic data reported by the Center for Engineering Strong Motion Data (CESMD) [28]. Figure 7 shows the seismic acceleration (g) of the Palekastro earthquake in 0° , 90° , and 360° directions. Figure 8 shows the displacement in 0° , 90° , and 360° directions. The maximum displacement occurred at 90° with a magnitude of 4.4096 cm. It has been observed that higher acceleration causes a more significant ground displacement.

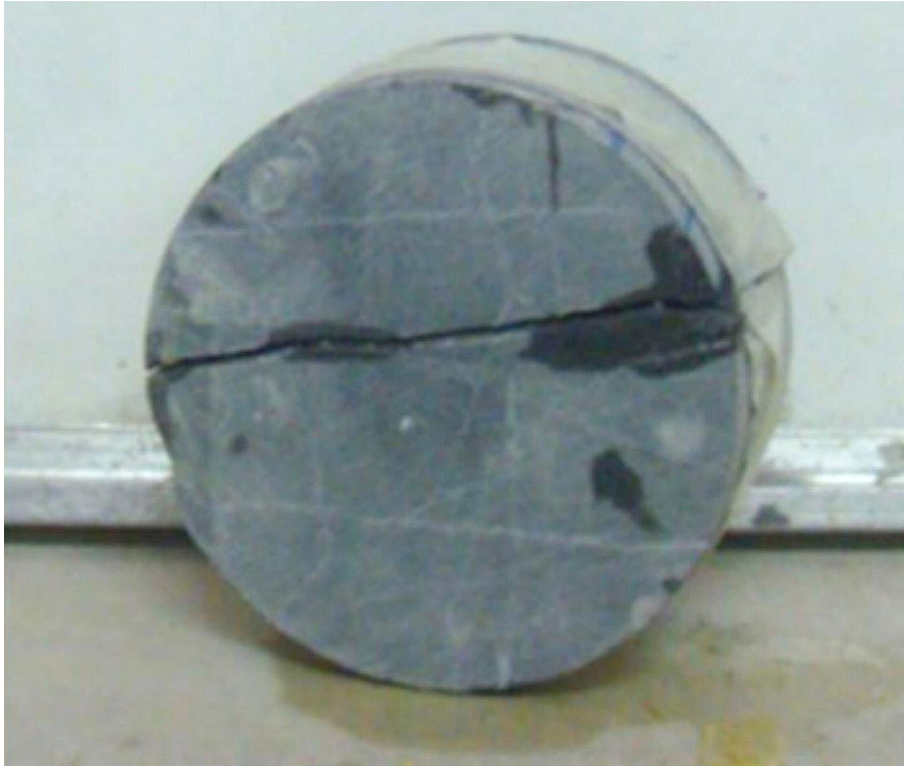


Fig. 4 The results of the Brazilian Tensile Strength (BTS) test on metasediment specimens [27]

Theoretical concept

Appropriate implementation of NXFEM is essential to obtain an acceptable result in nonlinear numerical simulation. It is necessary to apply the theoretical concept with simplified procedures to the ABAQUS procedures to analyze displacement, stress behavior, and strain magnitude in the crack and selected points of the simulated model.

The entire strain is taken into consideration for evaluating the crack stiffness by considering nonlinear elasticity, as presented in Eq. 1. Equations 2 and 3 were applied to find the crack path for a crack with a stress-free face. Equations 1–4 are J-integral, similar to Griffith's strain energy release rate. The J-integral can be obtained from the acceleration-displacement graph [29]. This integral illustrates the strain energy release rate in simulated cracked bedrock and the energy released around the crack. The theoretical concept of the current study investigates the crack path based on the strain energy density, and a stress-strain curve was used to analyze the nonlinear volumetric deformation of the rock model.

$$\frac{\epsilon_p}{\epsilon_y} = A \left[\frac{\sigma}{\sigma_y} \right]^N \quad (1)$$

$$J = \int_{\Gamma}^s [W dy - T \frac{\partial u}{\partial x}] ds \quad (2)$$

$$U = \frac{\text{Strain energy}}{\text{Unit volume}} = \int_0^{\epsilon} \sigma d\epsilon \quad (3)$$

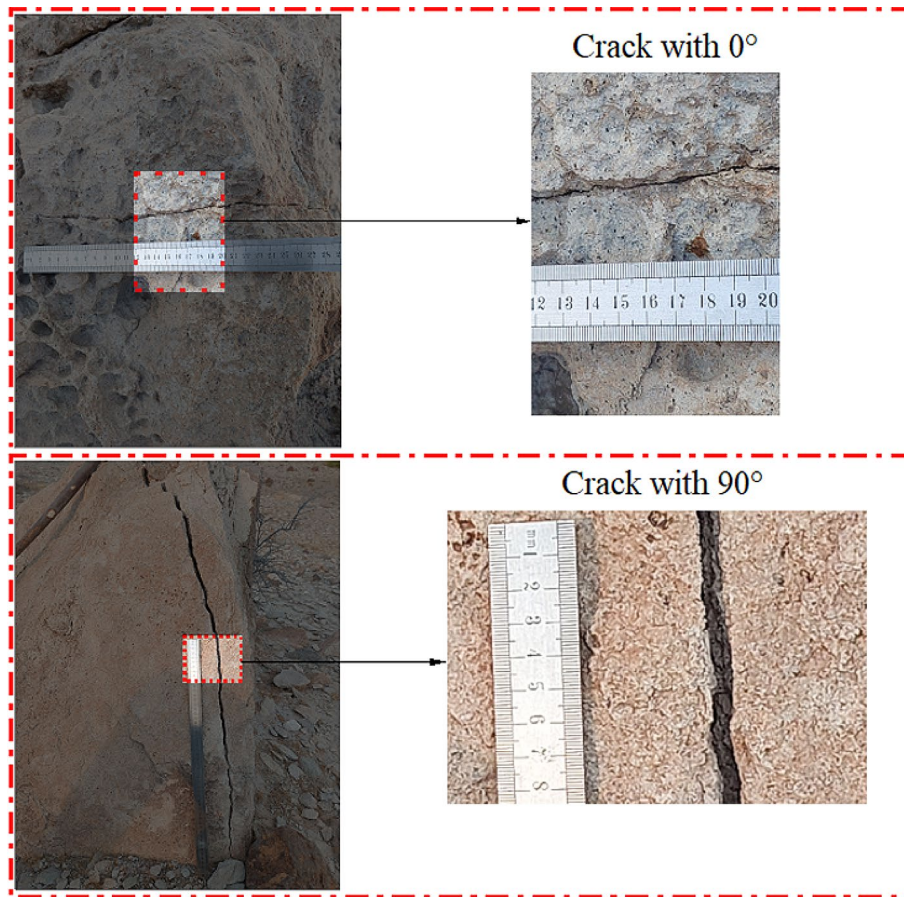


Fig. 5 Crack path propagation in the rock close to 0° and 90°

$$J = -\frac{dP}{da} (J/m^2) \quad (4)$$

The stress state around the crack is recognized as the stress intensity factor (SIF) and is represented in Eq. 5. The three main factors in calculating stress intensity are crack length, applied stress, and geometric correction coefficient. The Y of Eq. 6 is a dimensionless function representing the impact of crack length. The maximum, minimum, and range of the stress intensity factor are presented in Eqs. 7–9, respectively [30]. The stress intensity range is nonlinear and complex for a model subjected to seismic acceleration. With the application of seismic acceleration to the model, ABAQUS can identify maximum and minimum applied stress along a crack path in the model. With attention to the nature of seismic acceleration and the ability of ABAQUS to present maximum and minimum applied stress, by using the results of the nonlinear numerical simulation and using Eqs. 7–9, it is possible to obtain the maximum, minimum, and range of the stress intensity factor at a critical point of a model.

$$K = Y\sigma\sqrt{\pi a} \quad (5)$$

$$Y = f(a, W, \dots) \quad (6)$$

$$K_{max} = Y\sigma_{max}\sqrt{\pi a} \quad (7)$$

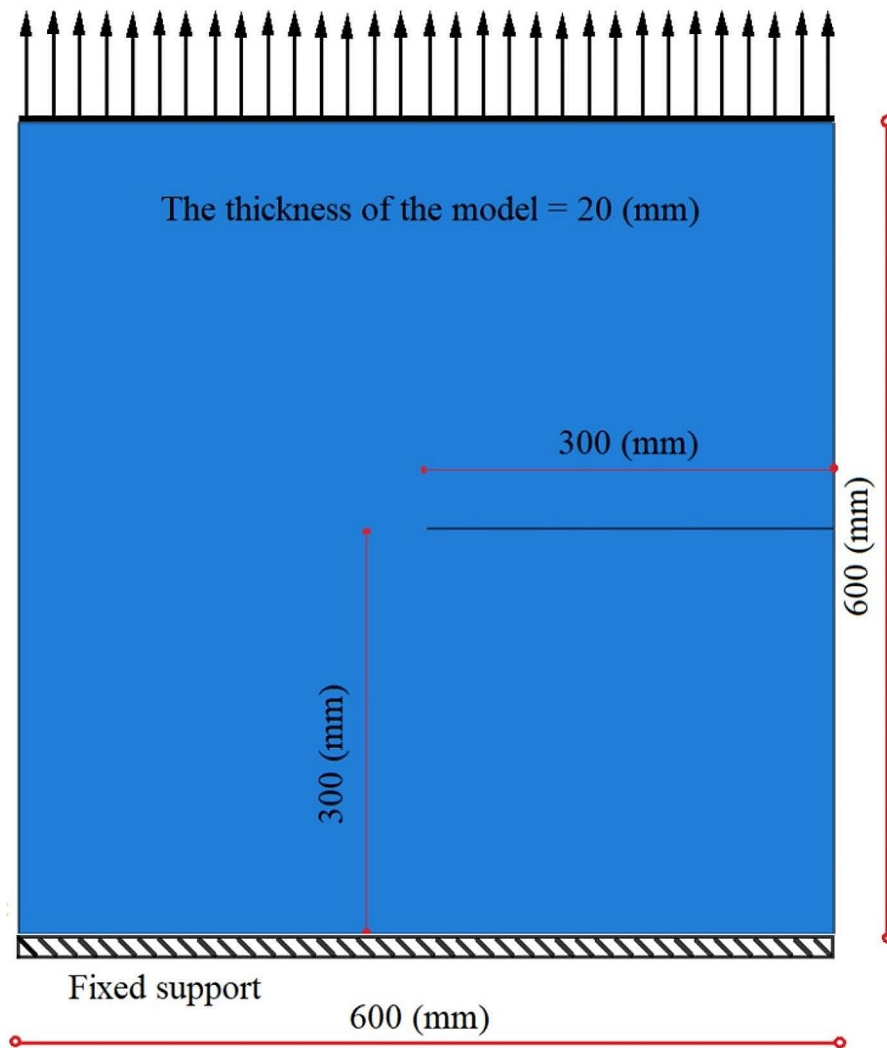


Fig. 6 Geometry and boundary condition of the model

$$K_{min} = Y \sigma_{min} \sqrt{\pi a} \quad (8)$$

$$\Delta K = K_{max} - K_{min} \quad (9)$$

When the crack propagates in the finite element solution, the stress intensity factor can be obtained using Eq. 10 [31].

$$K_I = \frac{E u_y}{4(1 - \nu^2)} \sqrt{\frac{2\pi}{r}} \quad (10)$$

The assumption is accepted based on crack growth in the center of the model. A critical step of numerical simulation includes the comparison of crack path morphology for each model. Seismic acceleration is applied to the model through a 3D fracture model. Fracture theory needs to be applied to numerical simulations using ABAQUS.

In accordance with the literature report [32], Eq. 11 is used to calculate displacement around the model crack in the X direction.

Table 2 The acceleration (g) and displacement (cm) were recorded in different earthquake stations [28]

Station	Distance (km) to the epicenter	Acceleration (g) peak			Displacement (cm)		
		0°	90°	360°	0°	90°	360°
Town Hall Siteia	13.6	-0.0894	-0.3432	0.1953	0.7744	4.4096	-2.1362
Lasithi Crete	91.2	0.0108	-0.0187	-0.0268	0.5171	-0.5099	-0.7366
NOA/RUB/GEO-FON Karpathos Greece							
Irakleio Crete Greece	108.5	0.0121	-0.0279	-0.0245	0.3477	0.7502	-0.7249
Sivas Crete Greece	133.0	0.0031	0.0077	0.0057	0.2532	0.2642	0.3047
Thera Santorini Greece	154.7	0.0064	0.0122	0.0112	0.136	0.4889	-0.3152
Mandraki Nisyros Greece	176.0	-0.0044	0.0075	0.0045	-0.2067	-0.3386	0.3301
Town Hall Rhodes Rhodes Island	226.1	0.0032	0.0054	0.0052	-0.2145	0.451	0.4385

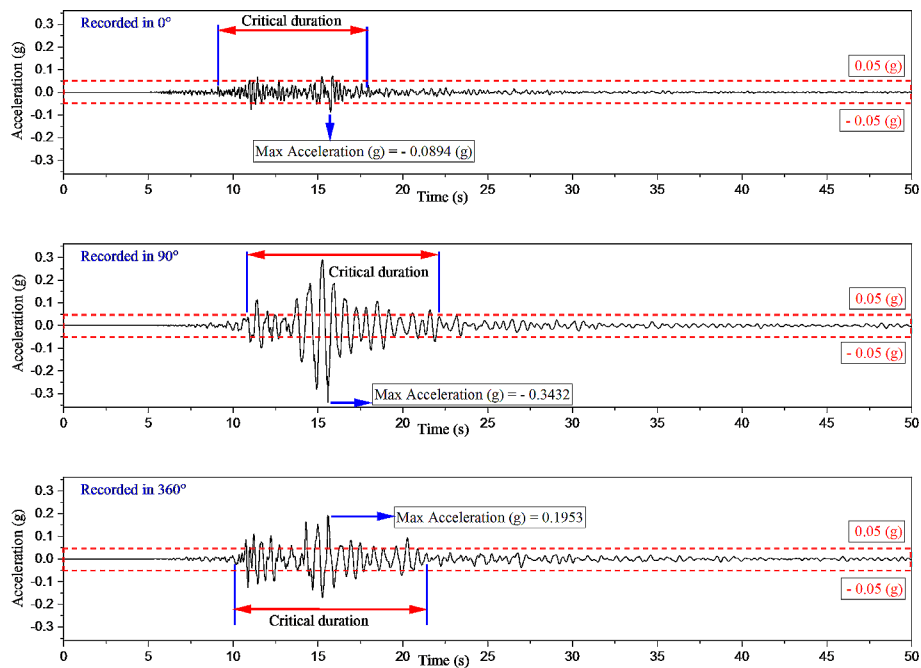


Fig. 7 The seismic acceleration of the Palekastro earthquake was applied to the model in the numerical simulation

$$u(r, \theta, t) = K_I(t) \frac{(1 + \nu)}{2E} \sqrt{\frac{r}{2\pi}} [(2k + 1) \sin \frac{\theta}{2} - \sin \frac{3\theta}{2}] \tag{11}$$

In 3D modeling, for any critical time, the SIF $K_I(t)$ can be obtained with reference to the displacement at two critical points of the model by using Eq. 12.

$$K_I(t) = \frac{E}{24(1 - \nu^2)} \sqrt{\frac{2\pi}{r_{OA}}} [8u(r_{OA}, + \pi, t) - u(r_{OB}, + \pi, t)] \tag{12}$$

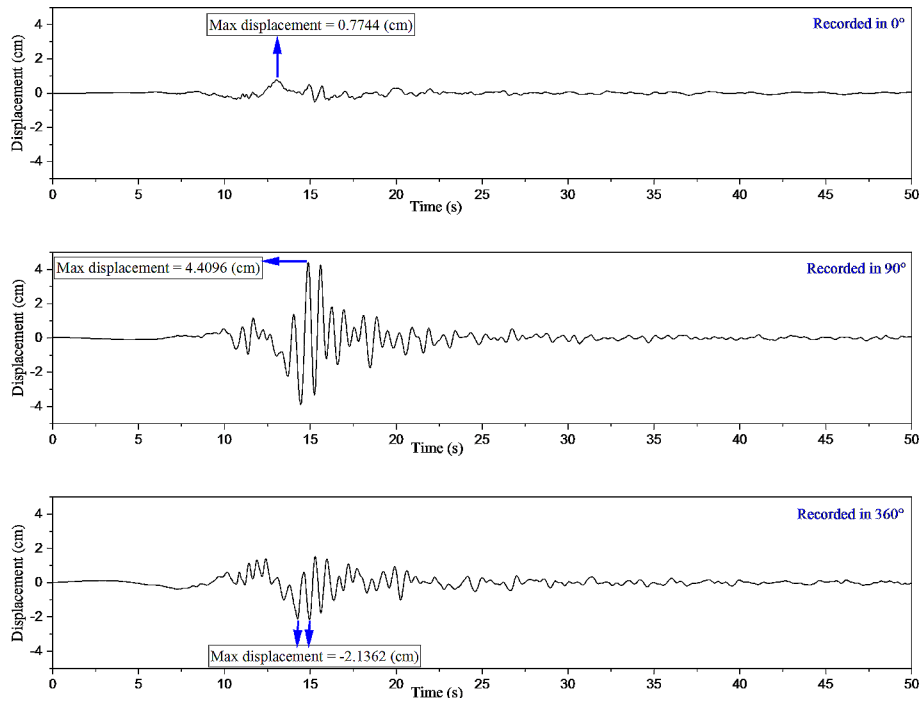


Fig. 8 The displacement (cm) of the Palekastro earthquake in 0°, 90°, and 360° directions

Statistical prediction procedure – ANNs

Different types of neural network models have been studied to predict several complicated engineering problems, including the seismic response of the earth's structure. These models include ANNs [17, 19 and 33–36], dictionary-based ROM nets [37], and polynomial matrix equations provided by machine-learning toolboxes [38].

Artificial neural networks (ANNs) were used to predict and compare the results with numerical simulation results. The ANNs are predictors based on the Levenberg-Marquardt back-propagation (LMBP) training algorithm. The inputs and outputs have been optimized with the LMBP algorithm to identify the impact of stress-causing strain on the model with respect to the mechanical properties of the model. The nodes (or layers of neurons), inputs, hidden layers, and outputs are ANN structures. Mathematical operations occur in the hidden layers and connect the inputs and outputs through the nodes. Two hidden layers were used in ANNs.

Equations 13–15 present the basic structure of the ANNs [36]. Where $x_1, x_2, x_3, \dots, x_n$ is the input, and $w_{k1}, w_{k2}, w_{k3}, \dots, w_{km}$ is the synaptic weight of neuron k in the ANNs structure and $\phi(*)$ represents the activation function. In addition, b_k represents the bias and the final output for neuron k is y_k . Based on the results of the mathematical procedures, the bias can be positive or negative. u_k and v_k refer to linear combiner output and activation potential, respectively. According to Eq. 14, v_k is the affine transformation to u_k through an artificial neuron mapping which is influenced by the bias of the ANNs.

$$u_k = \sum_{i=1}^n w_{ki}x_i \quad (13)$$

$$v_k = u_k + b_k \quad (14)$$

$$y_k = \phi(v_k) \quad (15)$$

Three types of activation functions can be used to solve nonlinear problems. The activation or transform function is presented in Eqs. 16–20 [39].

$$\phi(v) = \begin{cases} 1 & \text{if } v \geq 0 \\ 0 & \text{if } v < 0 \end{cases} \quad (16)$$

$$\phi(v) = \frac{1}{1 + e^{-av}} \quad (17)$$

$$\phi(v) = \tanh(v) = \frac{e^v - e^{-v}}{e^v + e^{-v}} \quad (18)$$

$$y_k = \begin{cases} 1 & \text{if } v_k \geq 0 \\ 0 & \text{if } v_k < 0 \end{cases} \quad (19)$$

$$y_k = \frac{1}{1 + e^{-av_k}} \quad (20)$$

The mean squared error (MSE) and regression value R are presented in Eqs. 21–22 [35]. MSE was used to measure error values in statistical analysis. MSE supports prediction quality. No error is considered if MSE equals zero. Based on the MSE and regression values, the accuracy of the produced data was evaluated from the nonlinear numerical simulation and compared to the theoretical concept. Statistical analysis was used to predict the accuracy of the strain when stress was applied in a nonlinear numerical simulation. Higher predictions can be expected if the regression value is closer to 1.

$$MSE = \frac{\sum_{i=1}^n (y_{mea} - y_{pre})^2}{n} \quad (21)$$

$$R^2 = 1 - \frac{\sum_{i=1}^n (Y_{mea} - Y_{pre})^2}{\sum_{i=1}^n (Y_{mea} - Y_{mean})^2} \quad (22)$$

Results and discussion

The cracks were extended based on the mechanical properties of the model. In addition, critical crack propagation results in the brittle occurrence of rock. Figure 9 shows crack propagation in models 1 and 2. There are two different morphologies of crack propagation in each model. The material's deformability governs the crack path. For nearly the same crack propagation length, model 2 has a lower strain. With reference to the modulus of elasticity of these two materials, the numerical simulation results have an excellent relationship with the theoretical concepts.

For the sandstone, comparing Fig. 5 with Fig. 9, the numerical simulation of crack propagation is very similar to what was observed in the field. When seismic loading is applied to the simulated models, the crack propagates and changes shape. Crack propagation depends on the mechanical properties of the materials. During the crack propagation, nonlinear volumetric deformation has two different morphologies along the crack path, as shown in Fig. 9. Numerical simulation can reveal the nonlinear volumetric deformation at each point in crack propagation. In the model of seismic simulation, the

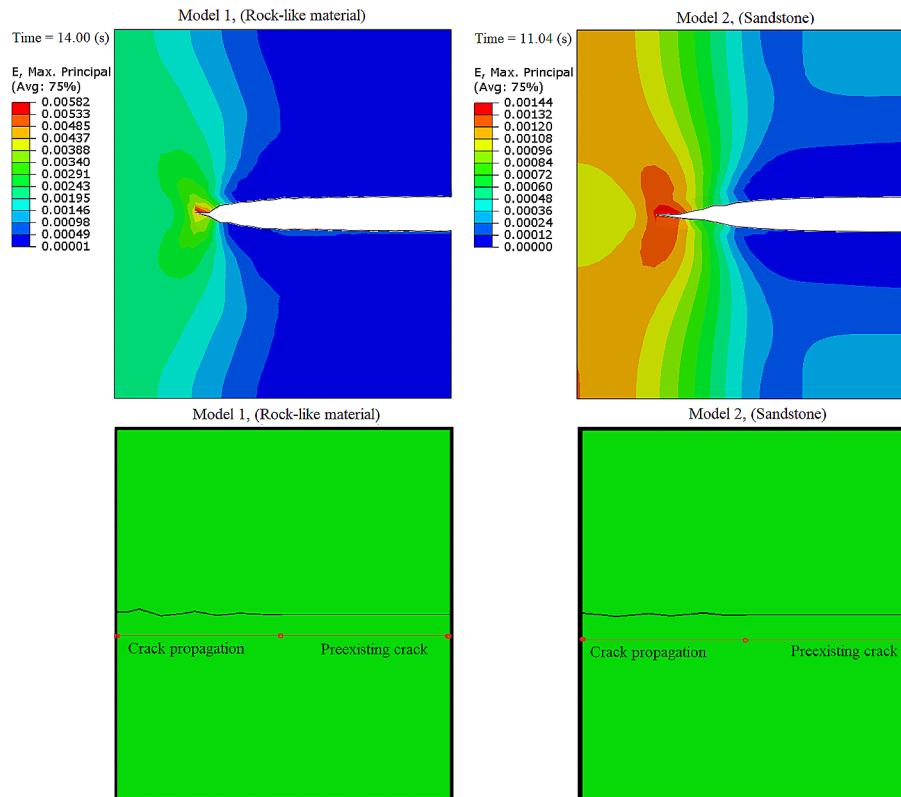


Fig. 9 The strain and crack propagation mechanism

multidirectional opening of the crack and the deformation of the models are associated with stress intensity paths and mechanical properties. The deformation in an open crack has a specific morphology for each model. In addition, the deformation at each stage of modeling is different for models 1 and 2. The deformation of the model is an important factor in crack propagation. When cyclic stress was applied to the model, the crack propagation direction and opening magnitude differed. This phenomenon is associated with the mechanical properties of the material. By comparing Figs. 5 and 9, it can be seen that crack propagation leads to deformation. There is a possibility that crack propagation and deformation have a direct relationship with the nature of seismic loading applied to the model.

When a dynamic strain is applied, the crack propagates straight. In addition, with no change in crack propagation speed under pure mode I, crack propagation has a constant increment rate [40]. According to the numerical simulation results in the present work, the crack propagates in a straight path in the mode I crack. Figure 9 shows that the crack propagation rate in sandstone occurs faster for an equal length of crack propagation in rock-like material and sandstone. In terms of the crack propagation mechanism, the findings of the present work agree well with those reported in the literature.

Based on the model boundary conditions, Fig. 10 illustrates the two points on the models used to assess displacement. Figure 11 shows displacement at nodes 519 and 1387 for models 1 and 2. The displacement interaction between the critical points and the development of crack paths is related to the model boundary condition. The mechanical properties of the materials govern the displacement at each point in the model. The displacement in Fig. 11 illustrates that the mechanical properties of materials play a critical

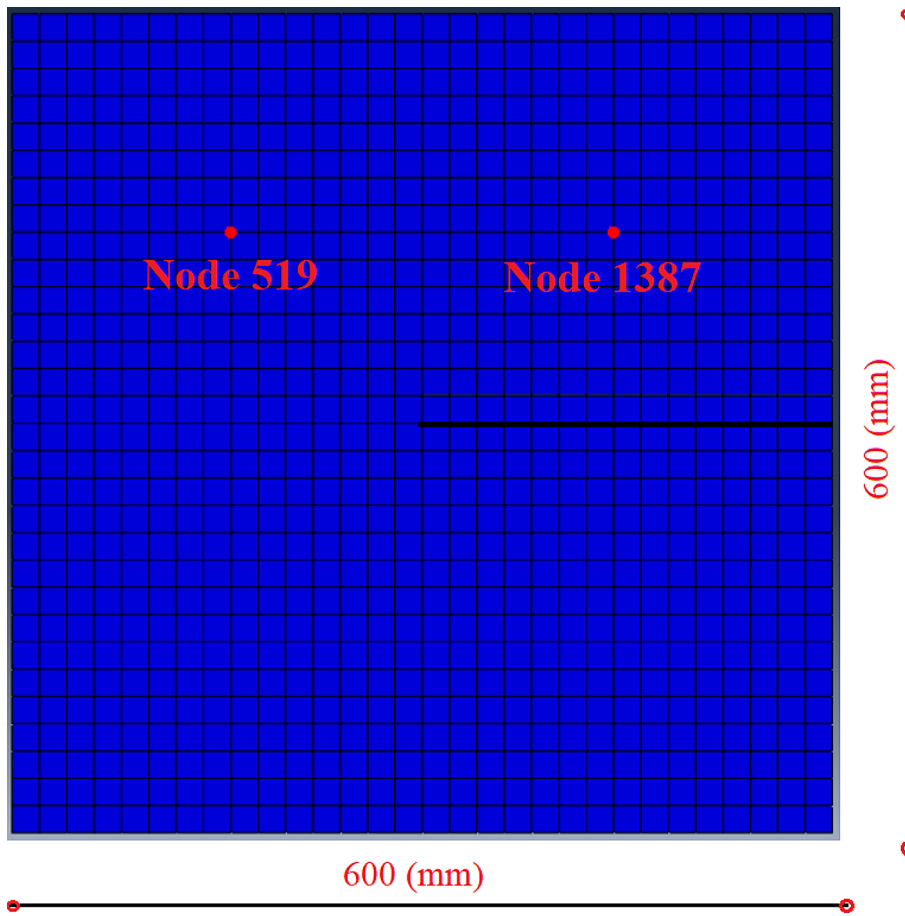


Fig. 10 The location of the nodes in the models 1 and 2

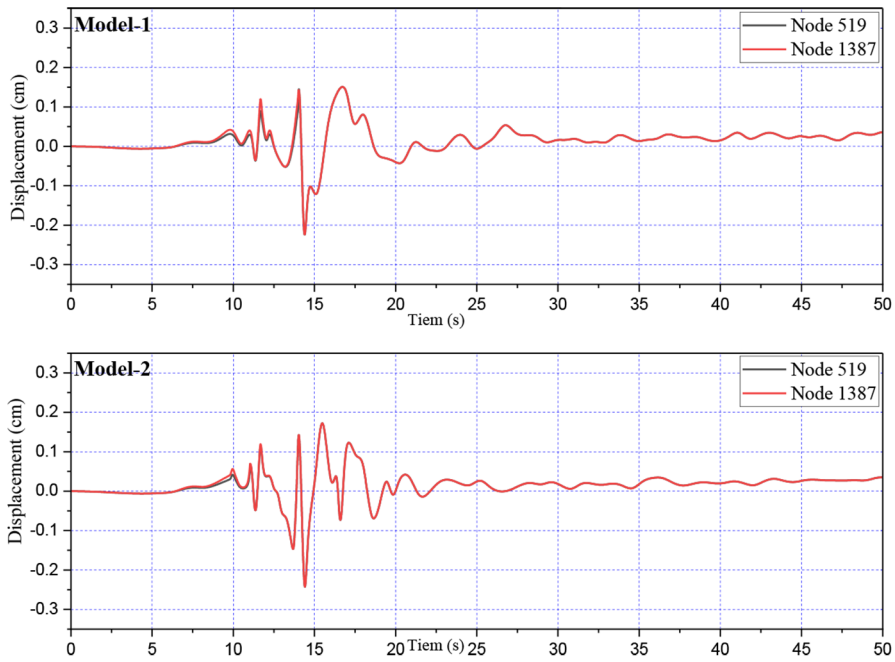


Fig. 11 The displacement in the selected nodes of models 1 and 2, by using NXFEM.

role in transferring loads in a model. Furthermore, the displacement in nodes 519 and 1387 for models 1 and 2 changes over time, and the displacement curve represents the vibration mechanism.

Figures 12 and 13 show the stress and strain fluctuation at two critical nodes of models 1 and 2. In sandstone, node 519 needs more loading for propagating the crack. The crack dissipates the seismic load while the rigid body transfers more seismic load in the model.

The model fails during the propagation of cracks in the shearing zone, which is located above an inclined shear crack line. Based on this concept, two points above the crack propagation path have been considered to analyze displacement and predict the failure mechanism of the model. The displacement relationship for all models at nodes 519 and 1387 is nonlinear. This study applied equal seismic loads to both models while the geometry and boundary conditions remained the same. Therefore, the mechanical properties of the material influence the stress, strain, and displacement curves. Due to material resistance, more load must be applied to the model to cause displacement.

The stresses and strains near the crack tip have been studied using numerical, analytical, and experimental methods, considering crack size [41]. The stress and strain along the crack path in rock-like material and sandstone were compared based on the length of the crack propagated at a specific stage. Figure 14 shows stress and strain along the crack in two segments along the pre-existing crack and the propagating crack, in accordance with Fig. 9. Stress and strain behave differently when mechanical properties change. A material's mechanical properties impact crack length, propagation, stress levels, and strain magnitudes. When seismic acceleration was applied, the material's brittleness impacted the model's collapse mechanism. In rock-like material, higher strain occurred than in sandstone, and the cracks propagated under lower stress. The seismic elastoplastic stress-strain results from the nonlinear numerical simulation are in consensus

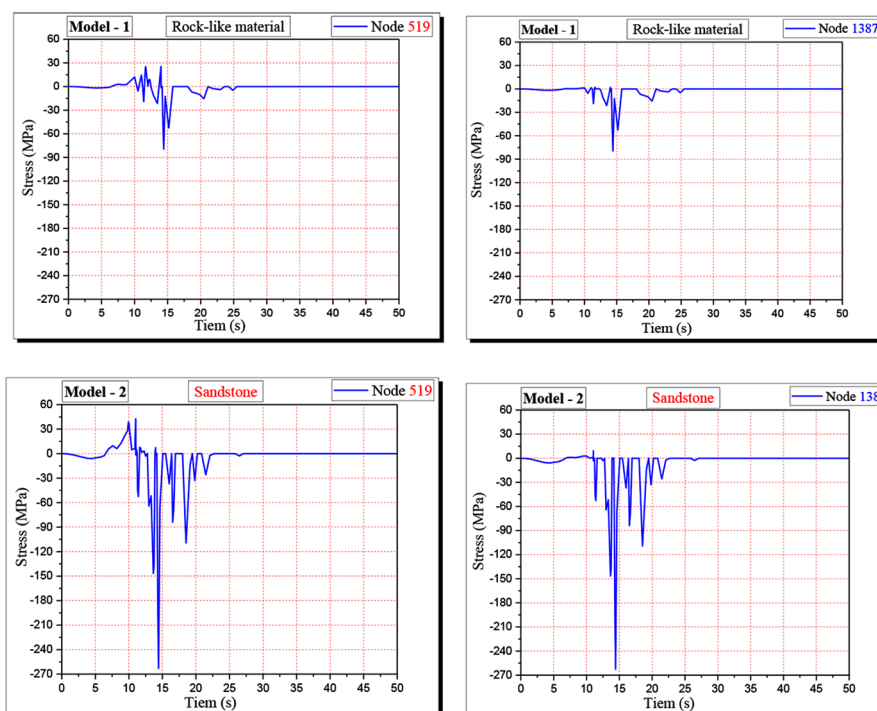


Fig. 12 The stress in the selected nodes of models 1 and 2, by using NXFEM.

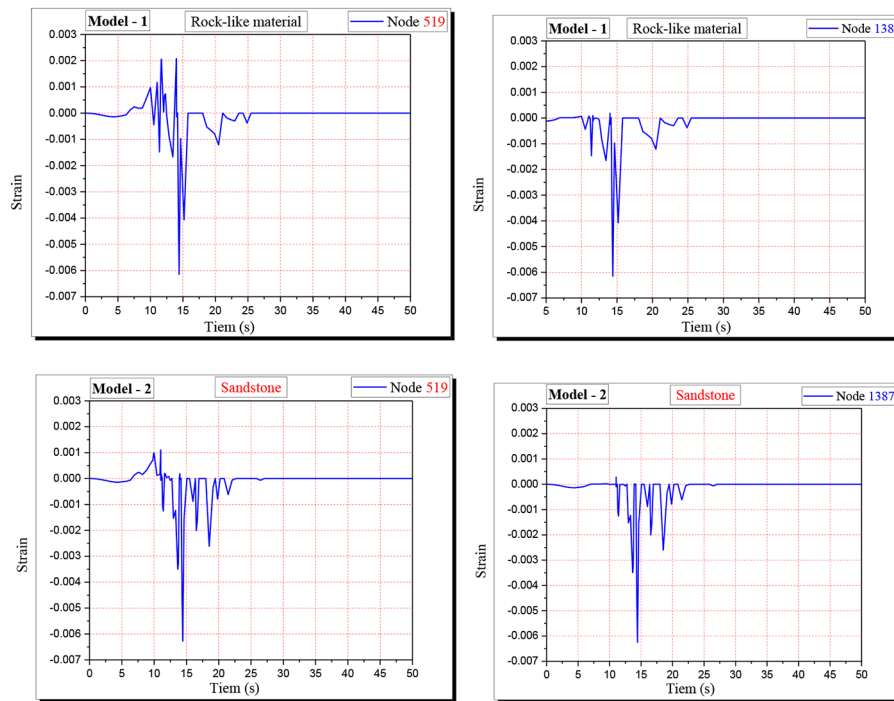


Fig. 13 The strain in two critical selected nodes of models 1 and 2

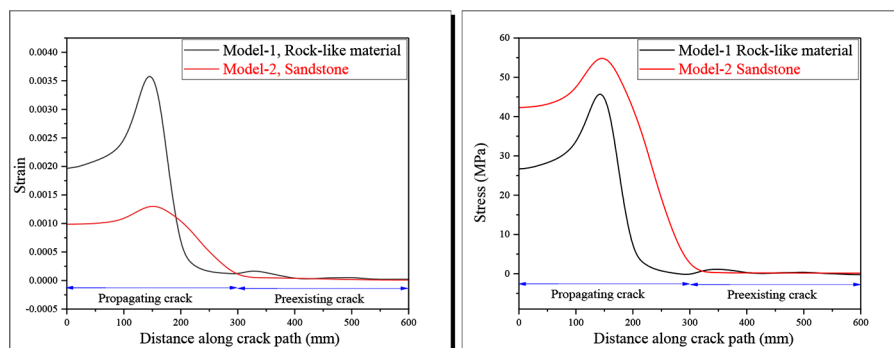


Fig. 14 The stress and strain distance along crack path, for preexisting and propagating parts of the crack

with the modulus of elasticity of sandstone and rock-like materials when the crack propagates.

In order to investigate the crack propagation on jointed rock, samples have been examined experimentally, and the results have been compared with numerical simulations. In numerical simulations, it was possible to identify the load response and failure mode that were difficult to observe in experimental investigations [42]. A numerical simulation can show the seismic response of a crack when it initiates and propagates.

Error estimation applied to fracture simulation was solved by using XFEM [43]. In the present investigation, the outcome of the ANN has been assessed by the coefficient of determination (R²), and mean squared error (MSE), and the prediction assessment is made for the simulation data produced by XFEM.

Displacement prediction by ANNs

Tables 3, 4, 5 and 6 present the data used in the ANNs. The histogram depicts the relative frequencies of training, validation, and test data. Figure 15 shows an error histogram with 20 bins in models 1 and 2 for all selected points. The center point of the histogram is a line that provides probability distributions. The line with zero error in both models was depicted for displacement probability distribution prediction.

Based on the comparison of the histograms between models 1 and 2, a different probability distribution in these two models can be observed at each selected point. However, the error line of prediction in model 2 looks more symmetric than in model (1) The error line has been drawn by comparing the target value with the prediction. Figure 11 shows the displacement at nodes 519 and 1387 for models 1 and (2) This prediction has been made using ANNs and is shown in Fig. 15.

Figure 16 shows regression analysis for displacement prediction in three stages: training, validation, testing, and a combination of the three stages. According to the regression analysis, R is 1 for all stages. This means a high level of prediction was done for models 1 and 2.

The R2 and MSE are calculated to assess the accuracy of the displacement forecast at the selected critical points. This process is performed on the dataset, randomly chosen

Table 3 Data used in ANNs for model 1 at node 519

No	Vertical Peak Stress (MPa)	Vertical Peak Strain	Tensile strength (MPa)	Vertical Displacement (mm)
1	-1.84935	-1.43226E-4	5.62	-0.06301
2	2.98455	2.39152E-4	5.62	-0.19475
3	-5.717	-4.42763E-4	5.62	-0.65126
4	14.5453	0.00117	5.62	0.85634
5	-19.1162	-0.00148	5.62	0.85961
6	24.8673	0.00201	5.62	0.88791
7	24.9441	0.00202	5.62	0.89536
8	24.8553	0.00203	5.62	0.02033
9	25.2387	0.00205	5.62	-0.73527
10	8.95407	7.31949E-4	5.62	1.00446
11	-21.527	-0.00167	5.62	1.10338
12	25.0213	0.00206	5.62	1.21547
13	25.0986	0.00208	5.62	1.22107
14	25.4578	9.29788E-4	5.62	1.26741
15	11.6572	7.8161E-4	5.62	1.26968
16	9.9234	8.25951E-4	5.62	1.40333
17	10.2058	8.65485E-4	5.62	1.36455
18	10.6093	6.92058E-4	5.62	1.46643
19	8.61144	-1.39861E-4	5.62	-2.74612
20	-1.48592	1.91589E-5	5.62	1.7271
21	0.20819	-0.00614	5.62	-0.53919
22	-79.3893	2.892E-7	5.62	-0.13295
23	0.00374	1.124E-7	5.62	-0.16773
24	0.00145	-0.00121	5.62	0.68068
25	-15.5876	-2.97518E-4	5.62	0.03779
26	-3.84399	6.55879E-8	5.62	0.04147
27	8.47244E-4	-3.75297E-4	5.62	0.0994
28	-4.8489	-5.59054E-8	5.62	0.1184
29	-7.22346E-4	-4.26699E-8	5.62	0.12625
30	-5.51228E-4	4.60651E-8	5.62	0.10138

Table 4 Data used in ANNs for model 1 at node 1387

No	Vertical Peak Stress (MPa)	Vertical Peak Strain	Tensile strength (MPa)	Vertical Displacement (mm)
1	-1.83191	-1.41639E-4	5.62	-0.0632
2	-5.66312	-4.37858E-4	5.62	-0.19535
3	1.67808	7.72669E-5	5.62	-0.65322
4	-18.9363	-0.00146	5.62	1.14961
5	2.0279	9.35119E-5	5.62	1.19342
6	1.42742	-1.03859E-4	5.62	1.19833
7	1.45929	3.85308E-5	5.62	0.02707
8	1.38334	3.30065E-5	5.62	-0.73696
9	0.912	-3.9875E-5	5.62	1.29612
10	-21.3698	-0.00165	5.62	1.35341
11	0.55551	3.54499E-5	5.62	1.36149
12	1.20518	-8.11111E-5	5.62	1.35455
13	1.15324	3.84979E-5	5.62	1.36675
14	-0.57667	-1.07531E-4	5.62	1.3888
15	-1.54559	-1.80492E-4	5.62	1.38344
16	1.21252	8.40745E-5	5.62	1.39696
17	-2.15196	-2.07468E-4	5.62	1.39461
18	1.35834	6.97317E-5	5.62	1.44526
19	-1.71964	-1.74302E-4	5.62	-2.74358
20	1.03903	6.90149E-5	5.62	1.7271
21	-1.48026	-1.70724E-4	5.62	-0.5387
22	1.53846	1.41413E-4	5.62	-0.13283
23	-1.9308	-2.03117E-4	5.62	-0.16758
24	1.99562	1.722E-4	5.62	0.03779
25	2.14698	1.83099E-4	5.62	0.04147
26	-2.79577	-2.48638E-4	5.62	0.0994
27	-79.539	-0.00615	5.62	0.1184
28	-15.6173	-0.00121	5.62	0.12625
29	-3.85132	-2.97947E-4	5.62	0.15637
30	-4.85815	-3.75838E-4	5.62	0.10138

Table 5 Data used in ANNs for model 2 at node 519

No	Vertical Peak Stress (MPa)	Vertical Peak Strain	Tensile strength (MPa)	Vertical Displacement (mm)
1	-5.98609	9.90714E-4	4	-0.06279
2	38.665	0.00111	4	0.42042
3	42.6658	2.20424E-4	4	0.05293
4	10.3113	2.28742E-4	4	0.69148
5	10.3113	2.08581E-4	4	0.69615
6	-52.5071	-0.00125	4	0.6589
7	7.75901	-0.00125	4	-0.56252
8	-146.613	1.99916E-4	4	1.14868
9	-146.613	-0.00153	4	-1.56298
10	-136.88	-0.00153	4	1.43378
11	7.34375	-0.0035	4	-2.80034
12	-83.8529	-0.0035	4	2.61987
13	-196.255	-0.00326	4	-0.89469
14	-262.311	-0.00201	4	1.72551
15	-262.311	-0.00467	4	-1.16519
16	-66.4312	-0.00627	4	0.48204
17	-36.9226	-0.00627	4	-0.35207

Table 5 Continued

No	Vertical Peak Stress (MPa)	Vertical Peak Strain	Tensile strength (MPa)	Vertical Displacement (mm)
18	-36.9226	-0.00158	4	0.50926
19	-83.8794	-8.78467E-4	4	-0.27477
20	-83.8794	-8.78467E-4	4	0.35419
21	-67.3782	-0.002	4	-0.02906
22	-109.146	-0.002	4	0.13551
23	-109.146	-0.0016	4	4.2287E-4
24	-14.3408	-0.0026	4	0.14058
25	-33.017	-0.0026	4	0.00535
26	-33.017	-3.41805E-4	4	0.35682
27	-25.7695	-7.88942E-4	4	0.1181
28	-25.7695	-7.88942E-4	4	0.19428
29	-2.72192	-6.1575E-4	4	0.11301
30	-2.72192	-6.1575E-4	4	0.33895

Table 6 Data used in ANNs for model 2 at node 1387

No	Vertical Peak Stress (MPa)	Vertical Peak Strain	Tensile strength (MPa)	Vertical Displacement (mm)
1	-5.9191	-1.4067E-4	4	-0.06305
2	2.79923	1.90417E-5	4	0.56854
3	2.1548	-5.47893E-6	4	0.07157
4	-3.01296	-5.90162E-5	4	0.69503
5	-1.35317	-9.76658E-5	4	0.69541
6	9.28222	1.11946E-4	4	0.69778
7	5.68434	-3.89539E-5	4	-0.56146
8	-0.4148	2.81835E-4	4	1.19453
9	-52.7023	1.41762E-4	4	-1.56275
10	-0.16996	-3.08451E-5	4	1.43199
11	-146.693	1.70399E-7	4	-2.79753
12	-0.78532	-0.00125	4	2.61987
13	0.40628	-1.64841E-5	4	-0.89378
14	-262.61	-0.00349	4	1.72551
15	0.00871	-1.65754E-5	4	-1.16402
16	-6.78348E-4	-2.47921E-5	4	0.48204
17	-36.9284	1.20771E-5	4	-0.35171
18	0.01638	-8.60812E-7	4	0.50926
19	-83.8915	-0.00625	4	-0.27449
20	0.00499	1.86488E-7	4	0.35419
21	-0.0028	-8.78707E-4	4	-0.02903
22	-0.00651	4.32779E-7	4	0.13551
23	-109.27	-0.002	4	4.22865E-4
24	0.00746	1.0771E-7	4	0.14058
25	-33.015	-1.54894E-7	4	0.00535
26	0.00361	-0.0026	4	0.35682
27	-25.7676	1.60873E-7	4	0.1181
28	0.00176	-7.85589E-4	4	0.19428
29	-2.72504	-6.13139E-4	4	0.11301
30	6.45962E-4	-6.48421E-5	4	0.33895

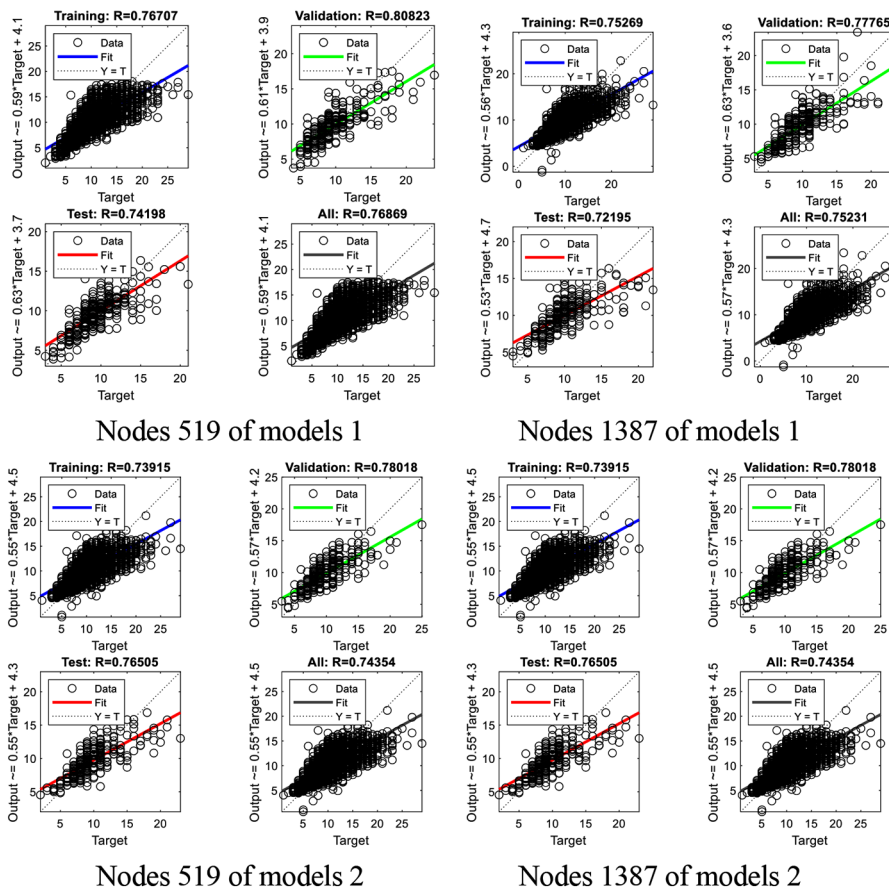


Fig. 15 The histogram for prediction of displacement in the nodes 519 and 1387 of models 1 and 2, by using ANNs

Table 7 The R^2 and MSE results

			Training	Validation	Test	Number of layers in ANNs
R^2	Model 1	Node 519	0.7671	0.8082	0.742	2
		Node 1387	0.7527	0.7777	0.722	2
	Model 2	Node 519	0.7391	0.7802	0.765	2
		Node 1387	0.7391	0.7802	0.765	2
MSE	Model 1	Node 519	4.3383	3.9022	3.5432	2
		Node 1387	4.5155	4.0977	4.9225	2
	Model 2	Node 519	4.7008	3.9719	4.6728	2
		Node 1387	4.7008	3.9719	4.6728	2

from several values obtained from nonlinear numerical simulations. In ANNs, appropriate layers must be selected to avoid overfitting and gradient disappearance. Two ANN layers were used to process output from input data. Table 7 illustrates the R^2 and MSE results. The MSE values for models 1 and 2 are acceptable. Figure 16 shows the function fit for output in models 1 and 2. The error in each model has different values. The ANNs generate multiple sets of data without impacting the original results. According to the fit and error for output element ANNs, models 1 and 2 have errors. Figure 16 presents the training targets, training outputs, validation targets, validation outputs, and test targets and outputs. The fit and error of the entire ANN are calculated based on these elements. Statistical analysis is an effective method to predict this kind of engineering problem. Figure 17 shows the statistical analysis of validation performances.

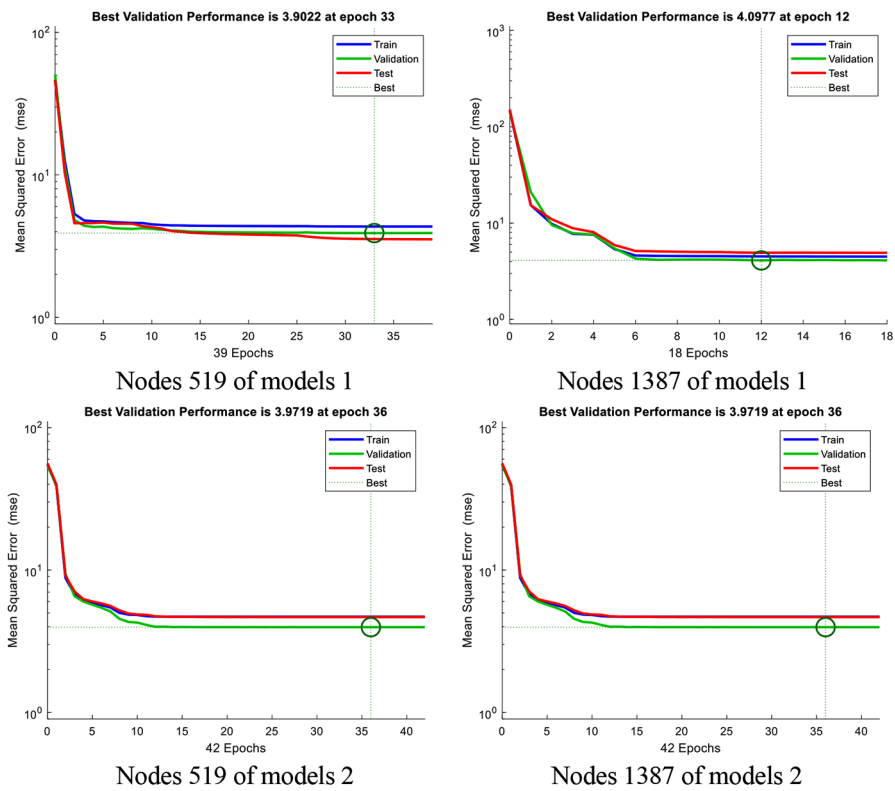


Fig. 16 The regression analysis for assessment prediction of displacement in the selected nodes of models 1 and 2, by using ANNs

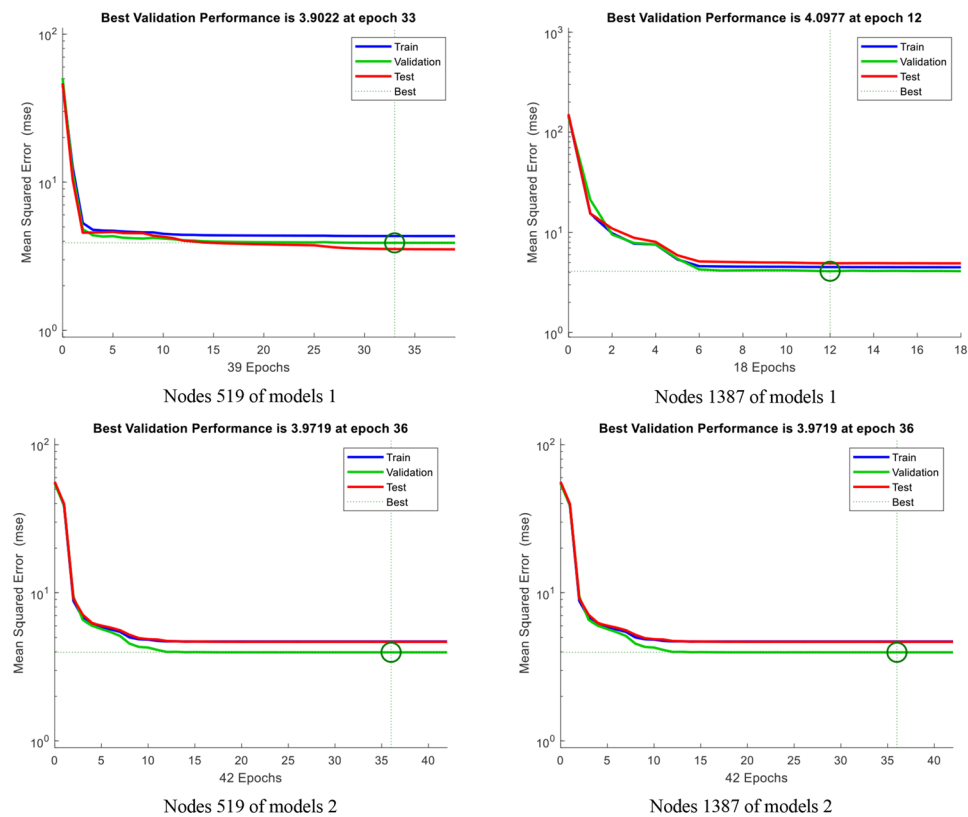


Fig. 17 The best validation performance for displacement prediction in the selected nodes of models 1 and 2, by using ANNs

The variance of error for training and prediction appeared to have a small value, and overfitting did not occur.

Conclusion

A nonlinear numerical simulation was conducted on rock-like material and sandstone to interpret the mechanisms of crack propagation in rock masses observed in the mountains. The prediction of displacement at the selected points of the models was made using nonlinear numerical simulation and Artificial Neural Networks (ANNs). Based on this investigation, the following conclusions have been drawn:

- Each material has a specific crack path, which can depend on several parameters. Crack path prediction was done for rock-like materials and sandstone with pre-existing cracks, considering the mechanical properties of the materials and seismic loading.
- To predict the stress-strain relationship along the crack path, NXFEM was used. The stress-strain relationship along the crack path is different for each material. Crack propagation, stress level, and strain magnitude are associated with material mechanical properties. In addition, the predicted results show that crack propagation in each material has a different mechanism.
- The model's boundary conditions were considered to identify critical points for analyzing the load-displacement relation of the model. The displacement at two critical points of models 1 and 2 has been studied and compared. Cracks dissipate seismic loads, whereas intact rock and rock bridges transfer seismic loads. The deformation of the model is a significant factor in crack propagation. The deformation along the crack path for each model has a different shape.
- At each point of the model, the mechanical properties of the materials control the displacement. According to the results of the numerical simulation in the mode I crack, in terms of the crack propagation mechanism, the present work's findings agree with those reported in the literature. Crack propagation occurs more rapidly for an equal length of crack propagation in rock-like material and sandstone. The speed of the crack changes according to the material's mechanical properties. The brittleness of the material changes the crack speed and shape.
- The seismic load causes the coalescence of the crack. Loading time history and spectrum characteristics are essential in the crack coalescence and propagation.
- Different types of loads and boundary conditions need to be investigated to minimize the overestimation of the elastoplastic stress and strain of a model.

Supplementary Information

The online version contains supplementary material available at <https://doi.org/10.1186/s40323-024-00261-7>.

Supplementary Material 1

Acknowledgements

The ADU authors acknowledge financial support from Abu Dhabi University's Office of Research and Sponsored Programs. The authors understand *Advanced Modeling and Simulation in Engineering Sciences* is an open access journal, and we should pay an article processing charge for the accepted article. We have read and understood the journal's policies, and we believe that neither the manuscript nor the study violates any of these.

Authors' information:

Authors' contributions

Omer Mughieda: Conceptualization; methodology; supervision; investigation; writing the draft, final review and editing. Lijie Guo: Formal analysis; methodology; data curation. Yunchao TANG: Investigation, methodology. Nader M. Okasha: Review, editing. Sayed Javid Azimi; Investigation, Software. Abdoullah Namdar: Software. Falak Azhar: Editing.

Funding

Not Applicable.

Data availability

Data are contained within this manuscript.

Declarations**Competing interests**

The authors declare no competing interests.

Omer Mughieda

Associate Professor Omer Mughieda is head of Department of Civil Engineering, Abu Dhabi University, Abu Dhabi, UAE. omer.mughieda@adu.ac.ae.

Professor Lijie Guo

Professor Lijie Guo is working at BGRIMM Technology Group, Beijing 100160, China. ljguo264@126.com.

Yunchao TANG

Professor Yunchao TANG is working at Key Laboratory of Disaster Prevention and Structural Safety of China Ministry of Education, School of Civil Engineering and Architecture, Guangxi University, Nanning, China 530004. joshua0115@gxu.edu.cn.

Professor Nader M. Okasha

Professor Nader M. Okasha is working at Department of Civil Engineering, College of Engineering, Abu Dhabi University, Al Ain, United Arab Emirates. nader.okasha@adu.ac.ae.

Mr. Sayed Javid Azimi

Mr. Sayed Javid Azimi is a lecturer at Structure Department, Engineering Faculty, International Islamic University of Afghanistan, Afghanistan. sjavidazimi@gmail.com.

Abdoullah Namdar

Dr. Abdoullah Namdar is a researcher at School of Civil Engineering, Iran University of Science and Technology (IUST), Narmak, Tehran, Iran. ab_namdar@yahoo.com.

Mrs. Falak Azhar

Mrs. Falak Azhar is an Independent Researcher, MSc Civil Engineering and Construction Management, Dubai, UAE. falakazhar95@gmail.com.

Nomenclature

u_y Displacement in a node

r Distances from the crack.

E Modulus of elasticity.

ν Poisson's ratio

K Stress intensity factors

K_I Stress intensity factors

s Arc length.

T External forces.

u Corresponding displacements.

ϵ_P Plastic strain

ϵ_y Yield strain

σ_y Yield stress

A Constant.

N Plastic stress-strain relationship.

U Strain energy density.

Γ Boundary

J - Integral.

a Length of the crack.

σ Applied stress

Y Geometric correction coefficient.

W Width of the component.

K_{max} Maximum stress intensity factor

K_{min} Minimum stress intensity factor

σ_{max} Maximum applied stress

σ_{min} Minimum applied stress

ΔK Stress intensity factor range

MSE Mean squared error

R^2 Regression value
 Y_{mea} Measured experimental
 Y_{mean} Mean of the measurements
 Y_{pre} Predicted data
 $x_1, x_2, x_3, \dots, x_n$ Input
 $w_{k1}, w_{k2}, w_{k3}, \dots, w_{km}$ Synaptic weight of neurons
 k Neurons
 $\phi (*)$ Activation function
 b_k Represents the bias
 y_k Output
 u_k Linear combiner output
 v_k Activation potential

Author details

¹Department of Civil Engineering, Abu Dhabi University, Abu Dhabi, UAE

²BGRIMM Technology Group, Beijing 100160, China

³Key Laboratory of Disaster Prevention and Structural Safety of China Ministry of Education, School of Civil Engineering and Architecture, Guangxi University, Nanning 530004, China

⁴Department of Civil Engineering, College of Engineering, Abu Dhabi University, Al Ain, United Arab Emirates

⁵Structure Department, Engineering Faculty, International Islamic University of Afghanistan, Afghanistan, Afghanistan

⁶School of Civil Engineering, Iran University of Science and Technology (IUST), Narmak, Tehran, Iran

⁷Independent Researcher, MSc Civil Engineering and Construction Management, Dubai, UAE

Received: 7 September 2023 / Accepted: 19 February 2024



References

- Mughieda O, Alzo'ubi AK. Fracture mechanisms of offset rock joints - a laboratory investigation. *Geotech Geol Eng.* 2004;22:545–62. <https://doi.org/10.1023/B:GEGE.0000047045.89857.06>.
- Mughieda O, Karasneh I. Coalescence of offset rock joints under biaxial loading. *Geotech Geol Eng.* 2006;24:985–99. <https://doi.org/10.1007/s10706-005-8352-0>.
- Mughieda O, Khawaldeh I. Scale effect on engineering properties of open non-persistent rock joints under uniaxial loading. *KAYAMEK'2004-VII Bölgesel Kaya Mekaniği Sempozyumu / ROCKMEC'2004-VIIth Reg Rock Mech Symp.* 2004;2004:Sivas-T.
- Namdar A, Berto F, Muhammad N. The displacement simulation for cracked earth structure with different geometry. *Procedia Struct Integr.* 2022;41(2022):394–402. <https://doi.org/10.1016/j.prostr.2022.05.045>.
- Namdar A, Karimpour-Fard M, Muhammad N. The seismic resistance simulation for cracked clayey backfill. *Eng Fail Anal.* 2022;106616. <https://doi.org/10.1016/j.engfailanal.2022.106616>. 140.
- Yan B, Kang H, Li X, Qi Q, Zhang B, Liu J. Damage constitutive model and mechanical properties of jointed rock mass under hydro-mechanical coupling. *Theoret Appl Fract Mech.* 2023;123:103735. <https://doi.org/10.1016/j.tafmec.2022.103735>.
- Wang C, Li Y, Dai F, Wu G, Yin F, Li K, Wang K. Experimental investigation on mechanical properties and failure mechanism of rock-like specimens containing an arc-shaped ice-filled flaw under uniaxial compression. *Theoret Appl Fract Mech.* 2022;119:103368. <https://doi.org/10.1016/j.tafmec.2022.103368>.
- Li Y, Cai W, Zhu W, Dong Z, Zhang Q. Particle flow analysis of parallel double crack evolution under uniaxial compression. *Zhongnan Daxue Xuebao (Ziran Kexue Ban) J Cent South Univ Sci Technol.* 2019;50:3035–45.
- Hooker JN, Gale JFW, Gomez LA, Laubach SE, Marrett R, Reed RM. Aperture-size scaling variations in a low-strain opening-mode fracture set, Cozzette Sandstone, Colorado. *J Struct Geol.* 2009;31(7):707–18. <https://doi.org/10.1016/j.jsg.2009.04.001>.
- Secor DT. Role of fluid pressure in jointing. *Am J Sci.* 1965;263:633–46. <https://doi.org/10.2475/ajs.263.8.633>.
- Segall P. Formation and growth of extensional fracture sets. *Geol Soc Am Bull.* 1984;95(4):454–62.
- Gudmundsson A. Fracture dimension, displacement and fluid transport. *J Struct Geol.* 2000;22:1221–31. [https://doi.org/10.1016/S0191-8141\(00\)00052-3](https://doi.org/10.1016/S0191-8141(00)00052-3).
- Gudmundsson A. Formation and growth of normal faults at the divergent plate boundary in Iceland. *Terra Nova.* 1992;4:464–71. <https://doi.org/10.1111/j.1365-3121.1992.tb00582.x>.
- Schultz RA. Displacement-length scaling for terrestrial and martian faults: implications for Valles Marineris and shallow planetary grabens. *J Geophys Res: Solid Earth.* 1997;102(6):12009–15. <https://doi.org/10.1029/97JB00751>.
- Niu Y, Zhou XP, Berto F. Evaluation of fracture mode classification in flawed red sandstone under uniaxial compression. *Theoret Appl Fract Mech.* 2020;107:102528. <https://doi.org/10.1016/j.tafmec.2020.102528>.
- Niu Y, Zhou XP, Berto F. Temporal dominant frequency evolution characteristics during the fracture process of flawed red sandstone. *Theoret Appl Fract Mech.* 2020;110:102838. <https://doi.org/10.1016/j.tafmec.2020.102838>.
- Namdar A. The forecasting bearing capacity of the mixed soil using artificial neural network. *Frattura ed Integrità Strutturale.* 2020;53:285–94. <https://doi.org/10.3221/IGF-ESIS.23.22>.
- Namdar A. The application of soil mixture in concrete footing design using linear regression analysis. *Mater Des P Mater Des Process Commun Recessing Commun (MDPC).* 2020;2020(e179). <https://doi.org/10.1002/mdp2.179>.
- Omar M, Shanableh A, Mughieda O, Arab M, Zeiada W, Al-Ruzouq R. Soils Found. 2018;58:1383–99. <https://doi.org/10.1016/j.sandf.2018.08.004>. Advanced mathematical models and their comparison to predict compaction properties of fine-grained soils from various physical properties.
- John R, Shah SP, Jenq Y. A fracture mechanics model to predict the rate sensitivity of mode I fracture for concrete. *Cem Concr Res.* 1987;17:249–62. [https://doi.org/10.1016/0008-8846\(87\)90108-6](https://doi.org/10.1016/0008-8846(87)90108-6).

21. Mughieda OS, Bani-Hani KA. Cracking of RC School Building due to Soil Expansion. *Jordan J Civil Eng.* 2007;1(4):393–408.
22. Namdar A, Darvishi E, Feng X, Zakaria I, Yahaya FM. Effect of flexural crack on plain concrete beam failure mechanism - A numerical simulation. *Frattura ed Integrità Strutturale.* 2016;36:168–81. <https://doi.org/10.3221/IGF-ESIS.36.17>.
23. Marsavina L, Iacoviello F, Pirvulescu D, Di Cocco L, Rusu V. L. (2019). Engineering prediction of fatigue strength for AM50 magnesium alloys. *Int. J. Fatigue* 127 (2019) 10–15. <https://doi.org/10.1016/j.jfatigue.2019.05.028>.
24. Bordonaro GG, Leardi R, Diviani L, Berto F. Design of experiment as a powerful tool when applying finite element Method: a case study on prediction of hot rolling process parameters. *Frattura ed Integrità Strutturale.* 2018;12(44):1–15.
25. Vantadori S, Ronchei C, Scorza D, Zanichelli A. Experimental tests and FE simulations to compute the mechanical and fracture properties of the shot-earth 772. *Fatigue Fract Eng Mater Struct.* 2023;46(1):49–62. <https://doi.org/10.1111/ffe.13846>.
26. Alzo'ubi AK, Martin CD, Mughieda OS. Numerical modeling of buckling rock movement. *Continuum and distinct element Numerical modeling in Geomechanics-2011.* Australia: Melbourne; 2011.
27. MGCE. Studies and rock mechanics designs of Azad pumped storage power plant. Iran: Mahab Ghodss Consulting Engineering Company; 2018.
28. Center for Engineering. Strong Motion Data (CESMD), <https://strongmotioncenter.org/>.
29. Cherepanov GP. The propagation of cracks in a continuous medium. *J Appl Math Mech.* 1967;31(3):503–12. [https://doi.org/10.1016/0021-8928\(67\)90034-2](https://doi.org/10.1016/0021-8928(67)90034-2).
30. Dowling NE. (2012). *Mechanical Behavior of Materials.* Boston, MA, United States, Pearson.
31. Cartwright DJ, Rooke DP. (1978). Evaluation of Stress Intensity Factors, A General Introduction to Fracture Mechanics. I. *Mech. Eng. Pub.*, 54–73.
32. Rose LRF. On the initial motion of a Griffith crack. *Int J Fract.* 1976;12(6):829–41. <https://doi.org/10.1007/BF00034622>.
33. Guo L, Li W, Namdar A. Using recycled aggregate for seismically monitoring of embankment-subsoil model. *Case Stud Constr Mater.* 2021;15(2021):e00605. <https://doi.org/10.1016/j.cscm.2021.e00605>.
34. Tang Y, Wang Y, Wu D, Liu Z, Zhang H, Zhu M, Chen Z, Sun J, Wang X. An experimental investigation and machine learning-based prediction for seismic performance of steel tubular column filled with recycled aggregate concrete. *Reviews Adv Mater Sci.* 2022;61:849–72. <https://doi.org/10.1515/rams-2022-0274>.
35. Shanmuganathan S, Samarasinghe S. S. (2016). Artificial Neural Network Modelling. 628. Cham. <https://doi.org/10.1007/978-3-319-28495-8>.
36. Haykin SS. *Neural networks and learning machines.* Volume 3. USA: Pearson Upper Saddle River, NJ; 2009.
37. Daniel T, Casenave F, Akkari N, Ryckelynck D. Model order reduction assisted by deep neural networks (ROM-net). *Adv Model Simul Eng Sci.* 2020;7:16. <https://doi.org/10.1186/s40323-020-00153-6>.
38. Groensfelder T, Giebel F, Geupel M, Schneider D, Jaeger R. Application of machine learning procedures for mechanical system modelling: capabilities and caveats to prediction-accuracy. *Adv Model Simul Eng Sci.* 2020;7:26. <https://doi.org/10.1186/s40323-020-00163-4>.
39. Patterson DW. *Artificial neural networks: theory and applications.* Prentice Hall PTR; 1998.
40. Alneasan M, Behnia M. Strain rate effects on the crack propagation speed under different loading modes (I, II and I/II): experimental investigations. *Eng Fract Mech.* 2021;258:108118. <https://doi.org/10.1016/j.engfracmech.2021.108118>.
41. Ribeiro V, Correia J, Mourao A, Lesiuk G, Gonçalves AD, Jesus A, Berto F. Fatigue crack growth modelling by means of the strain energy density-based Huffman model considering the residual stress effect. *Eng Fail Anal.* 2022;140:106543. <https://doi.org/10.1016/j.engfailanal.2022.106543>.
42. Alzo'ubi AK, Mughieda OS, Kewalramani M. (2023). Modeling of independent versus dependent tensile–frictional strength behavior of jointed rocks. *Geotechnical and Geological Engineering.* (2023). <https://doi.org/10.1007/s10706-023-02443-3>.
43. Panetier J, Ladeveze P, Chamoin L. Strict and effective bounds in goal-oriented error estimation applied to fracture mechanics problems solved with XFEM. *Int J Numer Methods Eng.* 2010;81(6):671–700. <https://doi.org/10.1002/nme.2705>.

Publisher's Note

Springer Nature remains neutral with regard to jurisdictional claims in published maps and institutional affiliations.